Chemistry Africa (2022) 5:827–839
https://doi.org/10.1007/s42250-022-00374-9

ORIGINAL ARTICLE

Efficient One-Pot Synthesis of Indolhydroxy Derivatives Catalyzed by $SnCl_2$, DFT Calculations and Docking Study

Yassine Hakmaoui[1] · Aslı Eşme[2] · Rahhal El Ajlaoui[1,3] · M. E. Belghiti[4] · Abdellah Zeroual[5] · El Mostapha Rakib[1]

Received: 4 January 2022 / Accepted: 27 April 2022 / Published online: 11 June 2022

Abstract
In this work we used an efficient and simple synthesis for the preparation of new indolhydroxy derivatives that has been performed by the reduction reaction of 2-nitrocinnamic acid or 2-nitrophenyl pyruvic acid with anhydrous stannous chloride ($SnCl_2$) as a metal catalyst in different alcoholic solvents. During this transformation there was the involvement of intramolecular elimination cyclization. In the case of the reduction of 2-nitrocinnamic acid we obtained hydroxyindole plus hydroxyquinoline, on the other hand, the reduction of 2-nitrophenyl pyruvic acid gives hydroxyindole only, the products were obtained in suitable yields. The structures of all the synthesized compounds were fully characterized by different spectroscopic techniques such as ^{1}H NMR, ^{13}C NMR. In addition, the obtained products have been tested in silico against anti-human immunodeficiency virus type 1 (HIV-1) and SARS-CoV-2 virus. The outcomes of this work are very promising to develop more efficient antiviral compounds, indicating that these products may be a probable drugs for the SARS-CoV-2.

Keywords 2-Nitrocinnamic acid · 2-Nitrophenyl pyruvic acid · Stannous chloride · Reduction · Antiviral compounds

1 Introduction

The Indole moiety is a subunit frequently found in pharmaceuticals with important biological and potent pharmacological activities [1–3], including anti-inflammatory [4, 5], anti-cancer [6–8], and anti-HIV [9–12] antagonistic activity inhibitor of kinase protein [13, 14]**.** Indole derivatives have recently invaded several areas of pharmacology and can be found in photosensitive cells [15]. Various methods for Indole preparation have been reported [16] due to the importance of Indoles in the pharmaceutical industry [17]. However, in the present work, we are interested in the synthesis of new Indole derivatives from the reduction of 2-nitrocinnamic and 2-nitrophenylpyruvic acid by $SnCl_2$ in different alcoholic solvents. In the last ten years, the reduction of nitroindazoles has been performed in the presence of $SnCl_2$ as a catalyst for these multiple advantages [18–24]. It is a better reducing agent in organic transformations because of its greater selectivity leading to the efficient syntheses of different heterocyclic compounds based on the reduction of nitro derivatives, more the simplicity of operation, non-corrosive, low cost and ease of isolation. In parallel, we have realized a docking study about Indole (benzopyrrole) against anti-human immunodeficiency virus type 1 (HIV-1) and SARS-CoV-2 virus. Thus, we have tested our products into the active sites of the HIV-1 Protease (PDB ID: 1HSG) and the SARS-CoV-2 main protease (M^{pro}) (PDB ID: 6LU7) proteins. Discovery Studio Visualizer software and PyMol were applied for the visualization of the docked compound. Its H-bond interactions and possible binding mode of the indole molecules with their target proteins, aiming to explain their antiviral activities.

✉ M. E. Belghiti
elbelghiti10@gmail.com

1 Laboratory of Molecular Chemistry, Materials and Catalysis, Faculty of Sciences and Technics, Sultan Moulay Slimane University, BP 523, Beni-Mellal, Morocco

2 Faculty of Education, Department of Elementary Science Education, Kocaeli University, 41380 UmuttepeKocaeli, Turkey

3 Department of Chemistry, Faculty of Applied Sciences Ait Melloul, IBN ZOHR University, N10, Cité Azrou, Ait Melloul, BP 6146,, 86150 Agadir, Morocco

4 Laboratory of Physical Chemistry of Materials, Ben M'Sick Faculty of Sciences, Hassan II University of Casablanca, Casablanca, Morocco

5 Molecular Modelling and Spectroscopy Research Team, Faculty of Science, Chouaïb Doukkali University, P.O. Box 20, 24000 El Jadida, Morocco

2 Results and Discussion

2.1 Synthesis

Based on the interest of our research group for the synthesis of nitrogenous compounds heterocycles [25] and following the work carried out on the reduction reactions of nitroheteroaryls, we are interested, in the present work in the synthesis of new derivatives of the indole from the reduction of 2-nitrocinnamic **1** and/or 2-nitrophenylpyruvic acid **4** by $SnCl_2$ in different alcoholic solvents (Scheme 1). The action of anhydrous tin chloride, in excess, in different alcoholic solvents on 2-nitrocinnamic acid **1** at the reflux of the alcohol, leads to a mixture of two products: hydroxyquinoline **3** and to new compounds of type 1-hydroxy-1H-indole-2-carboxylate **2a–f** (Scheme 1). The yields of compounds **2a–f** and **3** are listed in Table 1. Contrary to what was observed in the case of the reduction reaction of nitroindazoles by $SnCl_2$ in different alcoholic solvents and which allowed access alongside the corresponding amine to alkoxyaminoindazole derivatives, the reduction reaction of 2-nitrocinnamic acid **1** under the same conditions mentioned above results in a mixture of two products derived from indole and quinoline. This result shows that the nature of the structure plays a fundamental role in obtaining new heterocyclic systems.

All structures were determined by examination of their NMR data. Furthermore, the structures of product **2b** are unambiguously confirmed through single-crystal X-ray

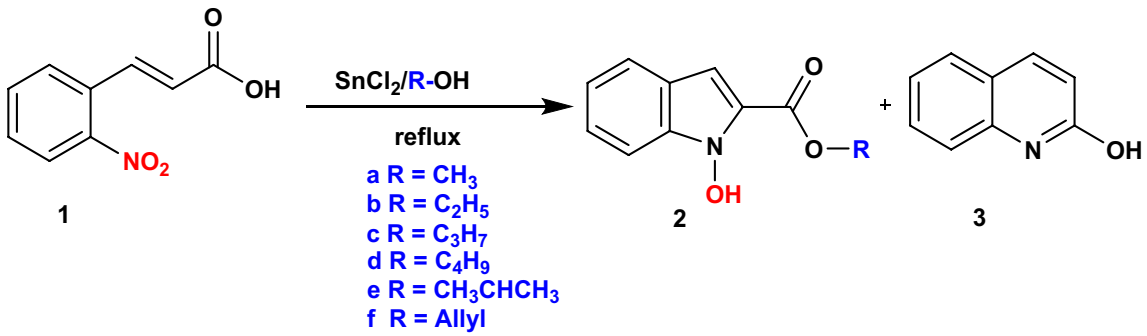

Scheme 1 Reaction of reduction of (E)-3-(2-nitrophenyl) acrylic acid by $SnCl_2$ in different alcoholic solvents

Table 1 Yields for N-alkyl-6-nitroindazoles 2a**–h** and **3a–h** hydroxyquinoline

System	Solvent	R	Reaction time (h)	Product 2a-f	Yields of 2a-f	Yields of 3
1	Methanol	CH_3	**8**	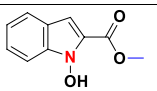	**2a** (55%)	40%
2	Ethanol	CH_2CH_3	**5**	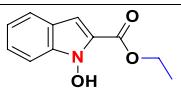	**2b** (54%)	42%
3	Propanol	$CH_2CH_2CH_3$	**6**	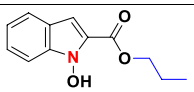	**2c** (50%)	40%
4	Butanol	$CH_2CH_2CH_2CH_3$	**8**	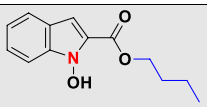	**2d** (54%)	43%
5	Propan-2-ol	$-CH(CH_3)_2$	**8**	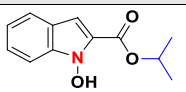	**2e** (47%)	38%
6	Prop-2-en-1-ol	Allyl	**8**	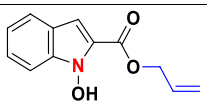	**2f** (60%)	(38%)

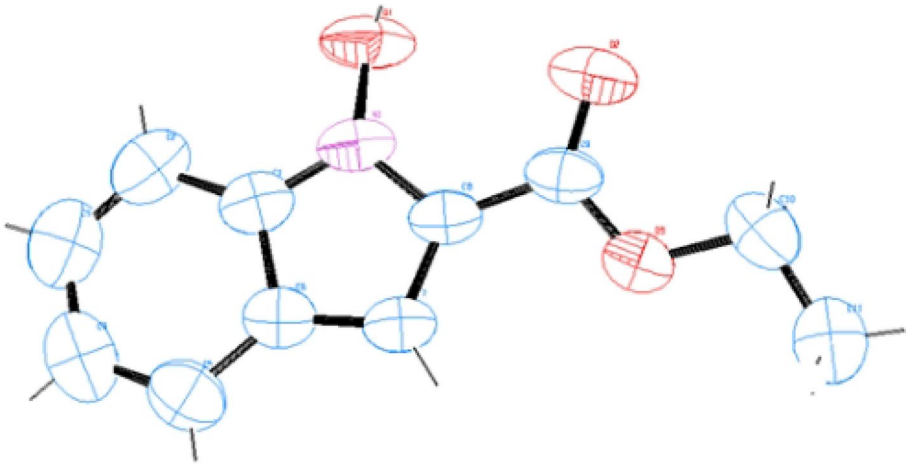

Fig. 1 X-ray crystal structures of **2b**

crystallographic analysis (Fig. 1). Looking at the influence that the solvent on the reduction/cyclization yields in the presence of $SnCl_2$ in different alcoholic solvents, we observed that the rearrangement resulting from the reduction of nitrocinamic acid is complete, the overall yield of the final products oscillating between 87% and 98%. The yields of N-hydroxyindoles **2a–f** are better compared to hydroxyquinoline **3**. Compound **2f** resulting from the reduction of nitrocinnamic acid in hydroxyalkyl is obtained in a better yield (60%).

In the ^{1}H NMR spectrum of compounds **2a–f**, we note more to the signals due to the protons of the alkoxy group, a signal at around 7.24–7.30 ppm attributable to the CH proton in position 3 of the indole and a signal at around 11.6–11.65 ppm of the proton of the hydroxy group OH. In the ^{13}C NMR spectrum of the compounds **2a–f**, we observe more to the signals due to the carbons of the alkoxy group, a signal around 109.2–110.0 ppm attributable to the CH carbon of the pyrrole.

A plausible mechanism for the formation of formation des N-hydroxyindoles **2a-f** and l'hydroxyquinoline **3**, Scheme 2. The initial step of the reduction reaction of compound **1** corresponds to the formation of esterified intermediate **A**. The latter evolves in two ways:

Way 1: A undergoes intramolecular cyclization, leading to the formation of intermediate **B**. The latter rearranges, and after aromatization leads to the expected products **2a-f.**

Way 2: The nitro group of **A** changes to the amine group of intermediate **C**, the latter undergo intramolecular cyclization and leads to the expected product **3**.

After this first interesting result of the synthesis of N-hydroxyindoles obtained for the first time via the reduction reaction of 2-nitrocinamic acid by $SnCl_2$ in different alcoholic solvents, we have opted to consider other

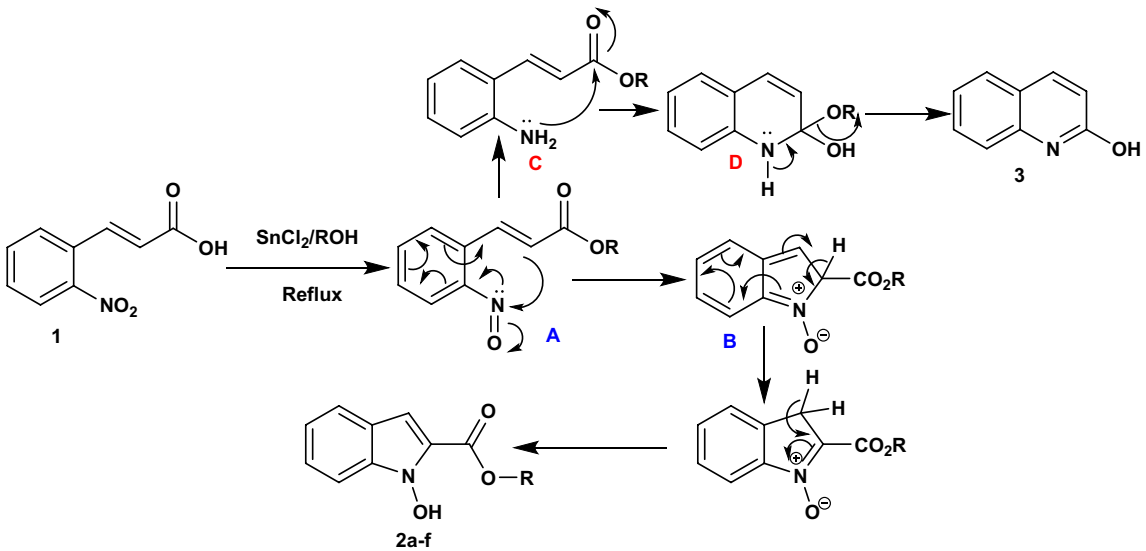

Scheme 2 Mechanism of reduction of (E)-3-(2-nitrophenyl) acrylic acid by $SnCl_2$ in alcohol

Table 2 Yield of products **2a** and **3** according to the number of $SnCl_2$ equivalents

Entry	Solvant	$SnCl_2$	Yield of **2a**	Yield of **3**
1	Methanol	1 eq	–	Trace
2	Methanol	2 eq	Trace	10%
3	Methanol	3 eq	55%	40%
4	Methanol	4 eq	30%	38%
5	Methanol	5 eq	Trace	30%

conditions to improve the yield of the hydroxyl indole derivatives. Therefore, the treatment of 2-nitrocinamic acid **1** with different equivalents of $SnCl_2$ in methanol permits obtaining N-hydroxy indole **2a** with varying yields (Table 2). The best yield is obtained with the use of three equivalents of $SnCl_2$. Beyond three equivalents of $SnCl_2$, product **3** is favoured.

We used the operating conditions mentioned above, this time in the presence of 2% HCl, the reduction reaction of nitrocinnamic acid with 3 equivalents of $SnCl_2$ led only to hydroxyquinoline **3** with a yield of 65% (Scheme 3).

In the reaction conditions similar to those developed previously, we also envisioned the reduction reaction of 2-nitrophenylpyruvic acid **4** with three equivalents of $SnCl_2$ at the reflux of ethanol. These conditions made it possible to obtain N-hydroxy indole **2b** with a yield of 60% (Scheme 4).

2.2 Experimental Part

Melting points were determined using a Büchi-Tottoli apparatus. ^1H and ^{13}C NMR spectra were recorded in DMSO-d_6, and solution (unless otherwise specified) with tetramethylsilane (TMS) as an internal reference using a Bruker AC 300 (^1H) or 75 MHz (^{13}C) instrument. The chemical shifts are given in ppm relative to tetramethylsilane (TMS) taken as an internal reference. The multiplicity of ^{13}C NMR resources was assigned by distortionless enhancement by polarization transfer (DEPT) experiments. Column chromatography was carried out on SiO_2 (silica gel 60Merck 0.063–0.200 mm). Thin-layer chromatography (TLC) was carried out on SiO_2 (silica gel 60, F 254 Merck 0.063–0.200 mm), and the spots were located with UV light. Commercial reagents were used without further purification unless stated. The general procedure for the synthesis of compound **2a–f** is as follows: under an inert atmosphere, (1.0 mmol) of 2-nitrocinnamic acid or (2-nitrophenylpyruvic acid) is added with $SnCl_2$ (3.0 mmol) in different alcoholic solvents (20 ml). The reaction mixture is brought to reflux for 6–8 h. After reduction, the solution was allowed to cool down. The pH was made slightly basic (pH 7–8) by the addition of 5% aqueous potassium bicarbonate before being extracted with ethyl acetate. The organic phase was washed with brine and dried over magnesium sulfate filtered and concentrated. The residue is eluted with ethyl acetate/hexane (10%/90%) through a column of silica gel.

Methyl 1-hydroxy-1H-indole-2-carboxylate 2a. White solid; mp 182–184 °C; **^{1}HNMR (DMSO-d_6):** δ3.78 (s, 3H; CH_3O), 6.48 (d, 1H, $J=9.2$ Hz, H-Ar), 7.13–7.23 (m, 3H, H-Ar), 7.26 (s, 1H, H-pyrrole), 7.84 (d, 1H, $J=9.2$ Hz, H-Ar), 11.63 (s, 1H, OH). **^{13}C NMR (DMSO-d_6):** 55.90 (CH_3O), 109.80 (CH), 116.80 (CH), 119.90 (CH), 120.1 (C), 122.80 (CH), 133.80 (C), 140.30 (CH), 154.50 (C), 162.00 (CO).

Ethyle 1-hydroxy-1H-indole-2-carboxylate 2b. White solid; mp 175–177 °C. **^{1}HNMR (DMSO-d_6):** δ1.33 (t, 3H, $J=7.20$ Hz, CH_3),4.03 (q, 1H, $J=7.20$ Hz, CH_2O), 6.48 (d, 1H, $J=9.60$ Hz, H-Ar), 7.11–7.22 (m, 2H, H-Ar), 7.25 (s, 1H, H-pyrrole), 7.83 (d, 1H, $J=9.6$ Hz, H-Ar), 11.63 (s, 1H, OH). **^{13}C NMR(DMSO-d_6):** 15.10 (CH_3), 63.80

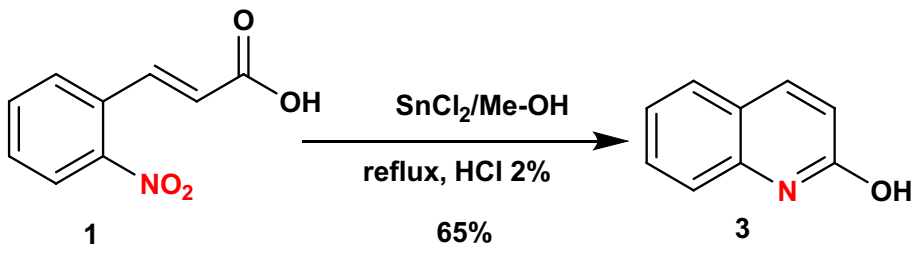

Scheme 3 The reduction reaction of nitrocinnamic acid with 3 equivalents of $SnCl_2$ in the presence of 2% HCl

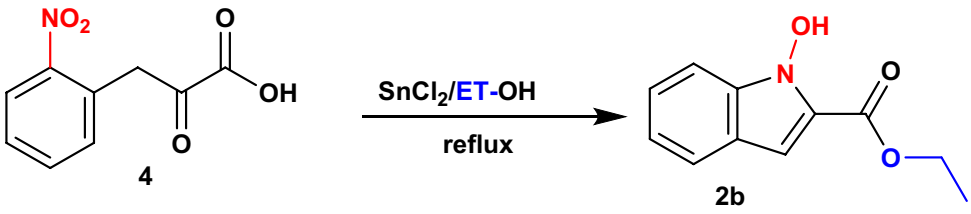

Scheme 4 The reduction reaction of 2-nitrophenylpyruvic acid with three equivalents of $SnCl_2$ at reflux of ethanol

(CH_2O), 110.50 (CH), 116.80 (CH), 120.10 (C), 120.30 (CH), 122.7 0(CH), 133.70 (C), 140.30 (CH), 153.80 (C), 162.00 (CO).

Propyle 1-hydroxy-1H-indole-2-carboxylate 2c. White solid; mp 170–172 °C. **^{1}HNMR(DMSO-d_6):** 0.98 (t, 3H, J = 7.40 Hz, CH_3), 1.68–1.79 (m, 2H, CH_2), 3.94 (t, 1H, J = 6.50 Hz, CH_2O), 6.48 (d, 1H, J = 9.60 Hz, H-Ar), 7.12–7.25 (m, 3H, H-Ar), 7.82 (d, 1H, J = 9.60 Hz, H-Ar), 11.63 (s, 1H, OH). **^{13}C NMR(DMSO-d_6):** 10.90 (CH_3), 22.50 (CH_2), 69.80 (CH_2O), 110.50 (CH), 116.80 (CH), 120.10 (C), 120.40 (CH), 122.70 (CH), 133.7 0(C), 140.30 (CH), 153.90 (C), 162.00 (CO).

Butyle 1-hydroxy-1H-indole-2-carboxylate 2d. White solid; mp 160-162 °C. **^{1}HNMR (DMSO-d_6):** 0.92 (t, 3H, J = 7.20 Hz, CH_3), 1.48–1.500(m, 2H, CH_2), 1.72–1.79 (m, 2H, CH_2), 3.96 (t, 1H, J = 6.90 Hz, CH_2O), 6.47 (d, 1H, J = 9.60 Hz, H-Ar), 7.10–7.24 (m, 3H, H-Ar), 7.84 (d, 1H, J = 9.6 Hz, H-Ar), 11.68 (s, 1H, OH). **RMN ^{13}C (DMSO-d_6):** 14.10 (CH_3), 19.20 (CH_2), 31.20 (CH_2), 68.00 (CH_2O), 110.50 (CH), 116.80 (CH), 120.30 (CH), 120.40 (C), 122.70 (CH), 133.70 (C), 140.30 (CH), 154.10 (C), 162.10 (CO).

Isopropyle 1-hydroxy-1H-indole-2-carboxylate 2e. White solid; mp 150–152 °C. **^{1}HNMR (DMSO-d_6):** 1.25 (d, 6H, J = 6.2 Hz, $2CH_3$), 4.57 (m, 1H, O-CH), 6.47 (d, 1H, J = 9.6 Hz, H-Ar), 7.09–7.24 (m, 3H, H-Ar), 7.80 (d, 1H, J = 9.6 Hz, H-Ar), 11.68 (s, 1H, OH). **RMN ^{13}C (DMSO-d_6):** 22.4 ($2CH_3$), 70.4 (CHO), 112.4 (CH), 116.8 (CH), 120.4 (C), 121.4 (CH), 122.6 (CH), 133.8 (C), 140.3 (CH), 152.7 (C), 162.1 (CO).

Allyl 1-hydroxy-1H-indole-2-carboxylate 2f. White solid; mp 195-197 °C. **^{1}HNMR (DMSO-d_6):** 4.55–4.58 (m, 2H; CH_2O), 5.33–5.38 (m, 2H, $=CH_2$), 5.98–6.10 (m, 1H, =CH), 6.480 (d, 1H, J = 9.60 Hz, H-Ar), 7.12–7.22 (m, 3H, H-Ar), 7.81 (d, 1H, J = 9.60 Hz, H-Ar), 11.62 (s, 1H, OH). **RMN ^{13}C (DMSO-d_6):** 69.10 (CH_2O), 103.70 (CH), 110.90 (CH), 117.90 ($=CH_2$), 120.20 (C), 120.40 (CH), 122.70 (CH), 134.10 (CH), 140.20 (CH), 153.60 (C), 162.10 (CO).

Quinolin-2-ol. White solid; mp 193-195 °C. **^{1}HNMR (DMSO-d_6):** 6.48–6.57 (m, 1H; H-Ar), 7.15 (dd, 1H, Ar-H), 7.48 (d, 1H, Ar-H), 7.63 (d, 1H, Ar-H), 7.87 (d, 1H, –CH=), 11.75 (s, 1H, OH). **RMN ^{13}C (DMSO-d_6):** 115.10 (CH), 119.10 (C), 121.70 (CH), 121.80 (CH), 127.80 (CH), 130.30 (CH), 138.80 (C), 140.10(CH), 161.90 (CO).

2.3 DFT Investigation

2.3.1 Calculation of the Global Reactivity Descriptors of 2b

All electron DFT geometry optimization, the spatial and electronic structure of the **2b** were performed by DFT/RB3LYP/6-31+G(d,p) basis set implemented in Gaussian 9, Revision C.01 [26] Density Functional Theory electronic structure program by combining the results of Gauss View 6.0.16 programs [27]. Calculated quantum chemical descriptors (QCD) were performed to study the structural and electronic properties of **2b**. The 3D minimized **2b** spatial structure and atom counts are shown in Fig. 2.

In this work, the SD (standard deviation) was operated in comparative studies between the minimized structure DFT method (bond length (in Å), bond angles and dihedral (in degrees)) in the isolated form and experimental results (X-ray data) for **2b** [28–31]. The average percentage change in link lengths between DFT data and X-ray data is 1% Å. The average percentage change in bond angles is 2% °. The average percentage change for the dihedrals is 1.7% °. Note that the link distances, link angles and dihedral angles calculated by the DFT/RB3LYP/6-31+G(d,p)/H_2O basis set are slightly high than the experimental (X-ray) observation. Indeed, theoretical calculations were made on a molecule in the aqueous phase, but the experimental data were obtained in the crystalline state. The crystal and ground state minimized structural descriptors of link distances, link angles and dihedral angles of **2b** are collected in Table 3.

The HOMO(TD-HOMO)/LUMO(TD-LUMO) orbital's and MEPs of **2b** using $DFT/RB3LYP/6-31+G(d,p)$ a basis set in the aqueous phase. DFT studies (local and global reactivity) covered geometry minimization. Frontier molecular orbitals the: HOMO (bonding orbital)–LUMO (anti-bonding orbital) energies and molecular electrostatic potential (MEPs) [32] is shown in Fig. 3.

The frontier molecular orbital (HOMO/LUMO) determine how the molecule interacts with other species. The HOMO (total density-HOMO) orbitals exhibited the predominance of the electron density character of the two characters (Sigma (σ) and Pi (π) bonds)) over the entire backbone of the compound. except for oxygen ($–O_{15}$ and $–O_{16}$) and carbon (C_{14}, C_{17} and C_{18}) atoms which exhibited of the electron density distribution (Sigma (σ) and Pi (π) bonds). On the other hand, the electron density distribution on the LUMO (total density-LUMO) orbitals showed a mixture of the two characters (Sigma (σ) and Pi (π) bonds) but the

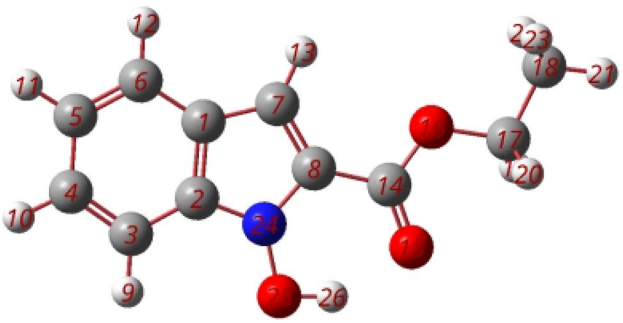

Fig. 2 3D-Minimized structure of **2b**

Table 3 Distances, angles and dihedral angles of **2b**

Bond length	DFT (Å)	X-ray data (Å)	Dihedral angles	X-ray data (◦)	DFT (◦)
R (1.2)	1.4336	1.434	**D (6.1.2.3)**	−0.0004	0.00
R (1.6)	1.4146	1.415	**D (6.1.2.24)**	–	180.00
R (1.7)	1.4215	1.422	**D (7.1.2.3)**	179.9997	180.011
R (2.3)	1.4066	1.407	**D (7.1.2.24)**	–	0.00008
R (2.24)	1.359	1.359	**D (2.1.6.5)**	0.0002	0.00001
R (3.4)	1.3864	1.386	**D (7.1.6.5)**	−179.9998	−180.00
R (4.5)	1.4216	1.422	**D (2.1.7.8)**	−179.9998	0.000048
R (5.6)	1.3852	1.385	**D (6.1.7.8)**	0.0001	−180.00
R (7.8)	1.3907	1.391	**D (1.2.3.4)**	0.0001	0.00002
R (8.14)	1.4556	1.456	**D (24.2.3.4)**	–	−180.0078
R (8.24)	1.3886	1.389	**D (1.2.24.8)**	–	0.00002
R (14.15)	1.2396	–	**D (1.2.24.25)**	–	180.0001
R (14.16)	1.3301	–	**D (3.2.24.8)**	–	−180.0012
R (16.17)	1.462	1.462	**D (3.2.24.25)**	–	0.00047
R (17.18)	1.5146	1.515	**D (2.3.4.5)**	−0.0001	0.000258
R (17.20)	1.0929	1.093	**D (3.4.5.6)**	0	0.00255
R (24.25)	1.3855	–	**D (4.5.6.1)**	0.0008	0.0015
			D (1.7.8.14)	–	–
			D (1.7.8.24)	–	−0.0019
			D (7.8.14.15)	–	−0.0001
			D (7.8.14.16)	–	180

Bond angles	DFT (◦)	X-ray data (◦)
A (2.1.6)	118.43	118.43
A (2.1.7)	107.52	107.52
A (6.1.7)	134.05	134.05
A (1.2.3)	122.79	122.79
A (2.3.4)	116.81	116.81
A (3.4.5)	121.72	121.30
A (4.5.6)	121.27	121.89
A (1.6.5)	118.98	121.72
A (1.7.8)	107.05	119.22
A (7.8.14)	132.47	–
A (7.8.24)	108.09	–
A (14.8.24)	119.44	–
A (8.14.15)	122.31	–
A (8.14.16)	113.86	–
A (15.14.16)	123.83	–
A (14.16.17)	117.40	–
A (16.17.18)	107.33	–
A (2.24.8)	110.76	–
A (2.24.25)	123.12	–
A (8.24.25)	126.11	–
A (1.2.24)	106.58	–

ethyl (–CH_2–CH_3) group did not show any type of electron density distribution.

2.3.2 Calculation of the Global Reactivity Descriptors of 2b.

The E_{HOMO} energy is found to be −5.04518 kcal/mol and the E_{LUMO} energy is found to be −1.67417 kcal/mol.

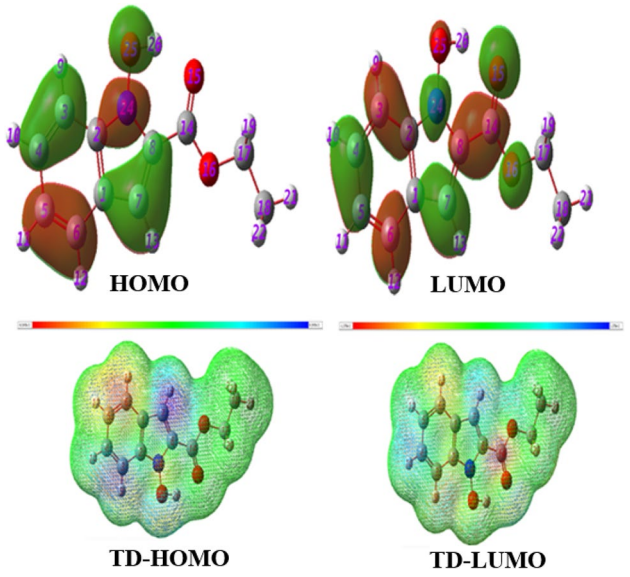

Fig. 3 The The HOMO (TD-HOMO). LUMO(TD-LUMO) plots of title **2b** molecule

Hence, the energy difference between E_{HOMO} and E_{LUMO} (energy gap ΔE_g) is + 3.37111 kcal/mol. The mostly small energy difference between HOMO and LUMO lead to the ease of transporting electrons from HOMO level to LUMO level. With a small gap, the molecule is more polarized and is known as a soft molecule [33]. The bond gap plays a critical role in determining the molecular electrical transport properties and enables us to determine the chemical reactivity and kinetic stability of the single molecule. A molecule with a lower ΔE_g energy is associated with a high chemical reactivity and low kinetic stability. The lower ΔE_g energy explains the charge transfer interactions taking place within the molecule, which was recently, used to prove the bio-activity from intramolecular charge transfer because it is an electron conductivity measure [34]. For the charged molecule, its value depends on the orientation and the choice of the origin of the molecule. This dipole moment value is among the descriptors useful for estimating the biological activity of molecule [33]. The relationships between biological activity and dipole (μ) moment value are studied in **2b** compound. The μ value of **2b** is again calculated using the DFT/RB3LYP/6-31+G(d,p) basis set. The μ value reflects the molecular charge distribution and is given as +3.80339D, which reflects the high stability of **2b**. The calculated (E_{HOMO}. E_{LUMO}. ΔE_g) values for these global reactivity descriptors using the DFT/*RB3LYP*/6 − 31 + G(d, p) basis set are displayed in Table 4.

2.3.3 Calculation of the Local Reactivity Descriptors of 2b

The mapping of 3D-MEPs gives an overview of the charge density of **2b** (Fig. 4). The greatest negative electrostatic potential is concentrated around the $\rangle N_{24} - O_{25} - H$. $\rangle C_{14} - O_{15}$. $\rangle C_{14} - O_{16}$ and $\rangle C_{17} - O_{16}$ groups and aromatic rings (red legend). As exposed in Fig. 3, this suggests that these (Sigma (σ) character of electron density distribution) groups and aromatic (Pi (π) character of electron density) ring are rich in electrons (correspond to their electron-withdrawing effect) and is most susceptible to electrophilic active centers. Regions with groups show a positive electrostatic potential (blue legend). which implies that they are deficient in electrons and are sensitive to nucleophilic active centers. The 3D-charge distributions on **2b** indicate that the molecule active (N_{24}, O_{25}, O_{16} and O_{15}) centres correspond to reactivity concerning electrophilic attack when the molecule loses electrons. On the other hand, the other centers correspond to reactivity concerning nucleophilic active centers.

From Fig. 4. the **2b** MEPs presence with colors scaled between -3.6610^{-2} (deepest red) and $+3.6610^{-2}$ (deepest blue). whereas the intermediary colors indicate the intermediary electrostatic potentials. The maximum negative electrostatic potential (electro-negativity) appears around the (=N_{24}, –O_{25}, –O_{16} and –O_{15}) atoms, which indicates the nucleophilic center reaction of the **2b** compound. On the other hand, the maximum positive electrostatic potential appears around the hydrogen atoms of the aromatic ring and some carbon atoms, which indicate the electrophilic site reaction of the **2b**. Applying the same ideas as before, the definitions for Fukui (local reactivity Fig. 5) Indices are [34]:

Nucleophilic (f^+) Fukui Function: $f_x^+ = \rho_{N+1}(x) - \rho_N(x)$

Electrophilic (f^-) Fukui Function: $f_x^- = \rho_N(x) - \rho_{N-1}(x)$

where $\rho_{N+1}(x)$. $\rho_N(x)$ and $\rho_{N-1}(x)$ are the electronic densities at point x for a system with $N+1$, N, and $N-1$ electrons. respectively.

The Fukui functions (electrophilic and nucleophilic regions) were calculated by the DFT/RB3LYP/6-31+G(d,p)/H_2O method to predict the chemical reactivity of the **2b**.

The nucleophilic active centre will be where the f^- value is maximal. In turn, the electrophilic active centre was controlled by the f^+ value. Therefore, the most favoured electrophilic active centres are C_{14}, $C_{7,}$ $O_{25,}$ O_{16} and O_{15}, and since the nucleophile index provides important values in N_{24}. Thus. for nucleophilic centre actives. The most reactive centres of **2b** are the rest of the carbons (C_1, C_2, C_{17}, C_{18}, C_5, …) atoms. this result is agreed with MEPs.

2.4 Molecular Docking

Indole (benzopyrrole) is one of the most widely distributed heterocyclic ring systems consisting of fused six-membered

Table 4 The obtained docking parameters of the (**2a–2f**) indole derivatives

Protein [PDB ID]		Bonded residues	Bond distances (Å)	Inhibition constant(μ M)	Intermolecular energy (kcal/mol)	Binding energy (kcal/mol)
1HSG	**2a**	ARG57	2.0	344.67	−5.62	−4.72
		GLU35	1.9			
		PRO79	3.5			
	2b	ARG57	1.9	328.39	−5.95	−4.75
		GLU35	1.9			
		PRO79	3.7			
	2c	ARG57	1.9	371.14	−6.17	−4.68
		GLU35	1.8			
		TRP42	4.0			
	2d	ARG57	2.1	222.21	−6.77	−4.98
		GLU35	1.8			
		PRO79	3.3			
	2e	ARG57	2.4	228.19	−6.16	−4.97
		GLU35	1.8			
		PRO79	3.6			
	2f	ARG57	2.1	420.98	−6.10	−4.61
		GLU35	1.7			
		LYS55	4.4			
6LU7	**2a**	THR111	3.6	49.77	−6.77	−5.87
		THR111	1.8			
		THR292	2.1			
		PHE294	3.4			
	2b	THR111	3.8	40.92	−7.18	−5.99
		GLN110	2.2			
		THR292	2.1			
		PHE294	4.0			
	2c	THR111	3.6	61.40	−7.24	−5.75
		THR111	2.9			
		THR292	2.2			
		PRO293	4.6			
	2d	ASN151	1.9	116.92	−7.15	−5.36
		THR292	2.1			
		GLN110	2.8			
		THR111	4.0			
		VAL104	4.5			
	2e	THR111	3.3	86.32	−6.74	−5.54
		THR111	2.6			
		THR292	2.2			
		PHE294	3.8			
	2f	THR111	3.6	54.46	−7.31	−5.82
		THR111	2.4			
		THR292	2.1			
		PRO293	4.7			

benzene and five-membered pyrrole rings. Indole containing compounds are well known to exhibit a variety of pharmacological activities such as anti-inflammatory [35], antioxidant [36], antiviral [37], antibacterial [38, 39], and anticancer [39], On the other hand, 2.3-dioxindole an oxidized form of Indole, is reported to exhibit a variety of biological activities like antibacterial, antimicrobial [41] and anti-human immunodeficiency virus type 1 (HIV-1) activities [42]. The

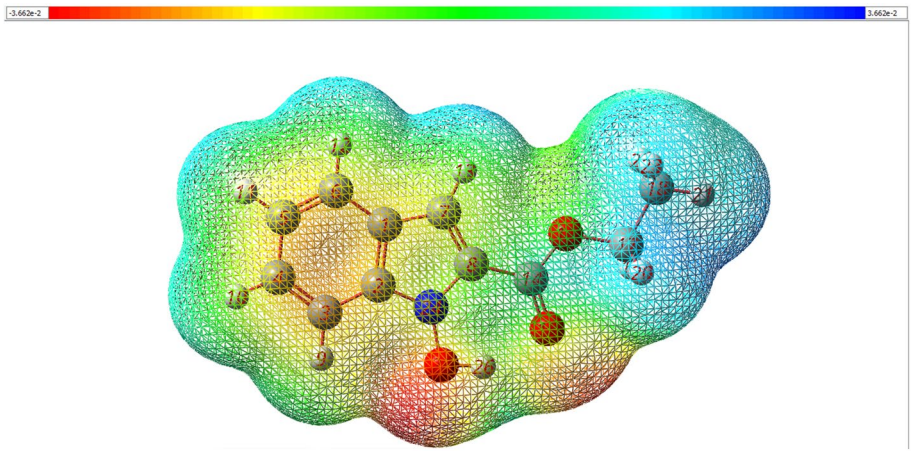

Fig. 4 3D-Molecular electrostatic potential(MEPs) surface of **2b**

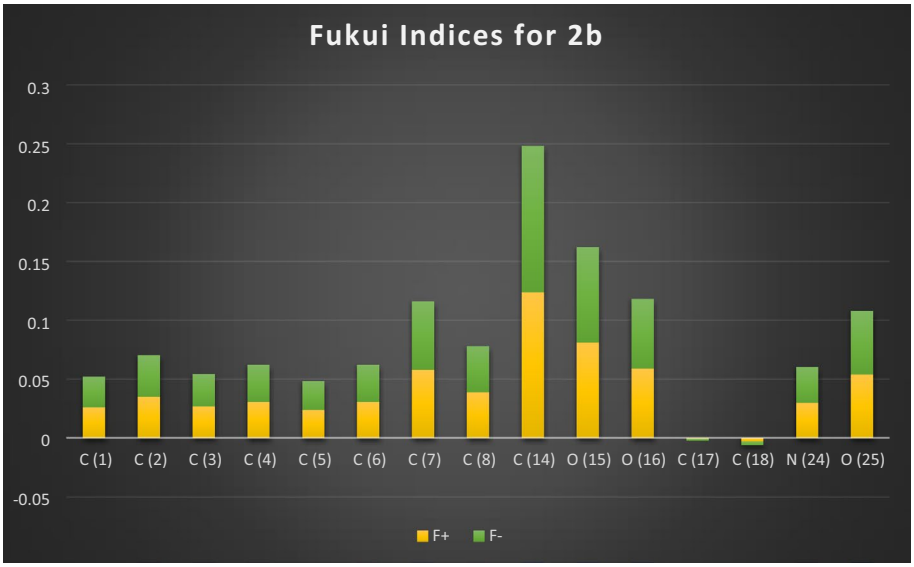

Fig. 5 The bar graph of Fukui (local reactivity) indices for nucleophilic f^- and electrophilic f^+ active centres for **2b**

structures of 1-hydroxy-1H-indole-2-carboxylate derivatives (**2a–2f**) evaluated were optimized using the Gaussian 9, software program [26]. The three-dimension crystal structures of the target proteins before docking were obtained from Protein Data Bank (see http//www.rcsb.org/pdb). The molecular docking study carried out with Autodock 4.2 program along with the graphical interface Auto Dock Tools (ADT) version 1.5.6 [43] was used to evaluate the potential of the (**2a–2f**) derivatives to docked into the active sites of the HIV-1 Protease (PDB ID: 1HSG) and the SARS-CoV-2 main protease (M^{pro}) of Coronavirus disease 2019 (PDB ID: 6LU7) proteins. Discovery Studio Visualizer software was applied to visually verify the docked compound and its H-bond interactions [44]. PyMol [45] was used to show the possible binding mode of the indole molecules with their target proteins, aiming to explain their anti-HIV-1 and antiviral activities. The water molecules were removed from the 1HSG and 6LU7 proteins. Polar hydrogen atoms and then Kollman and Gasteiger atom charges were added to the (**2a**–**2f**) derivatives by Auto dock Tools (ADT) before subjecting to docking analysis.

Auto Dock binding energy (kcal/mol). inhibition constants (μM), and interactions of all the docked compounds with protein residues were listed in Table 5. 1HSG crystal structure of the HIV-1 Protease bound with binding ener gy – 4.72, – 4.75, – 4.68, – 4.98, – 4.97, – 4.61 kcal/mol for **2a, 2b, 2c, 2d, 2e** and **2f** respectively. The trend of the human immunodeficiency virus type 1 activity of all the indole derivatives is as follows: **2d > 2e > 2b > 2a > 2c > 2f**. Interaction of anti-HIV-1 protein shows the existence of many interactions which are as follows: two conventional hydrogen bonds and one Pi-Alkyl bond was found in 1HSG interacting with amino acids (1.9–2.4 Å, ARG57;

Table 5 The E_{HOMO}, E_{LUMO}, ΔE_g as well as other global reactivity descriptors of **2b**

Properties	Chemical descriptors	Values
HOMO energy (Kcal/mol)	E_{HOMO}	−5.04518
LUMO energy (Kcal/mol)	E_{LUMO}	−1.67417
Bond gap (Kcal/mol)	$\Delta E_g = E_{HOMO} - E_{LUMO}$	+3.37111
Ionization potential (Kcal/mol)	$I = -E_{HOMO}$	+5.04518
Electron affinity (Kcal/mol)	$A = -E_{LUMO}$	+1.67410
Dipole Moment (Debye)	μ	+3.80339
Electronic total energy (Ha)	E_{TOTAL}	−706.233

1.7–1.9, GLU35 and 3.3–3.6, PRO79) with the inhibition constant (228.19–420.98 Mμ). respectively, The antiviral activity of the (**2a–2f**) indole derivatives obeyed the order **2b > 2a > 2f > 2c > 2e > 2d**. Several interactions between COVID-19 main protease (PDB ID: 6LU7) and **(2a–2f)** indole derived compounds are as follows: the conventional hydrogen bond interaction between indole ring and THR111 residue is observed within the bond distance 3.3–3.8 Å and Pi-Alkyl interactions between PHE294, PRO293, VAL104 residues and hydrogen atom of CH_3 group at 3.4–4.7 Å. It can be observed in Figs. 6 and 7 that hydrogen and oxygen atoms in the (**2a–2f**) indole derivatives are responsible for forming hydrogen bonds with 1HSG and 6LU7 protein residues.

3 Conclusion

In conclusion, we have developed a new rapid and efficient synthesis strategy allowing access to various derivatives of N-hydroxyindole and hydroxyquinoline. Our strategy involves the condensation reaction intramolecular reductive in different alcoholic solvents of 2-nitrocinnamic acid and 2-nitrophenylpyruvic acid. This reduction reaction with stannous chloride ($SnCl_2$) gave good yields with a short reaction time and easy processing. This method represents a new strategy for obtaining new derivatives of substituted indole, which promises a wide application of organic, biological and pharmacological products. Finally, this reduction made it possible to isolate the substituted indole by a judicious choice of the metal catalyst with better yields, which enriches the database of the literature. The docking results about our Indole products show an interesting potential of them against anti-human immunodeficiency virus type 1 (HIV-1) and SARS-CoV-2 virus.

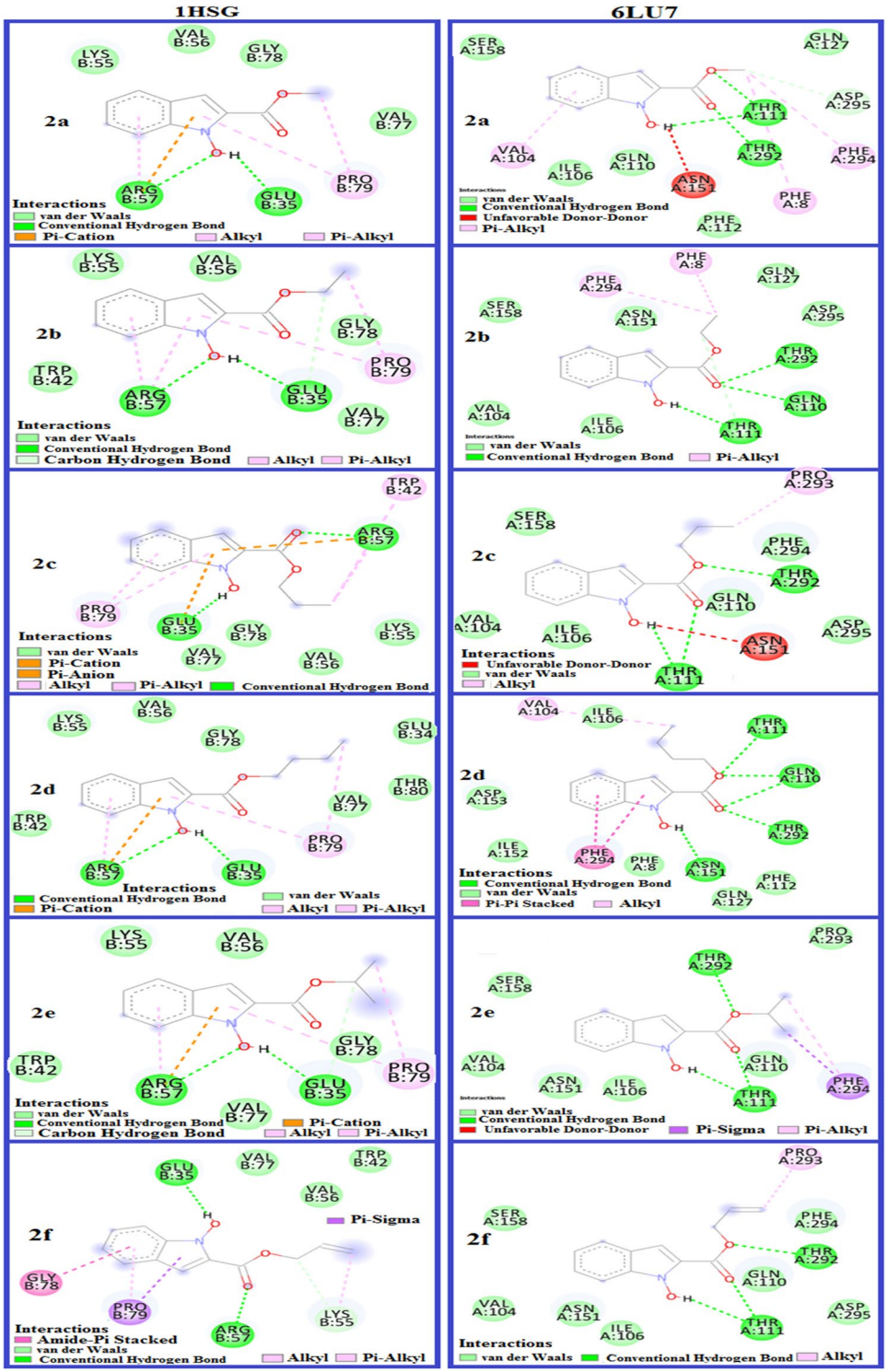

Fig. 6 2D diagrams of the (**2a–2f**) indole derivatives docked into the binding site of the anti-HIV-1 and antiviral proteins

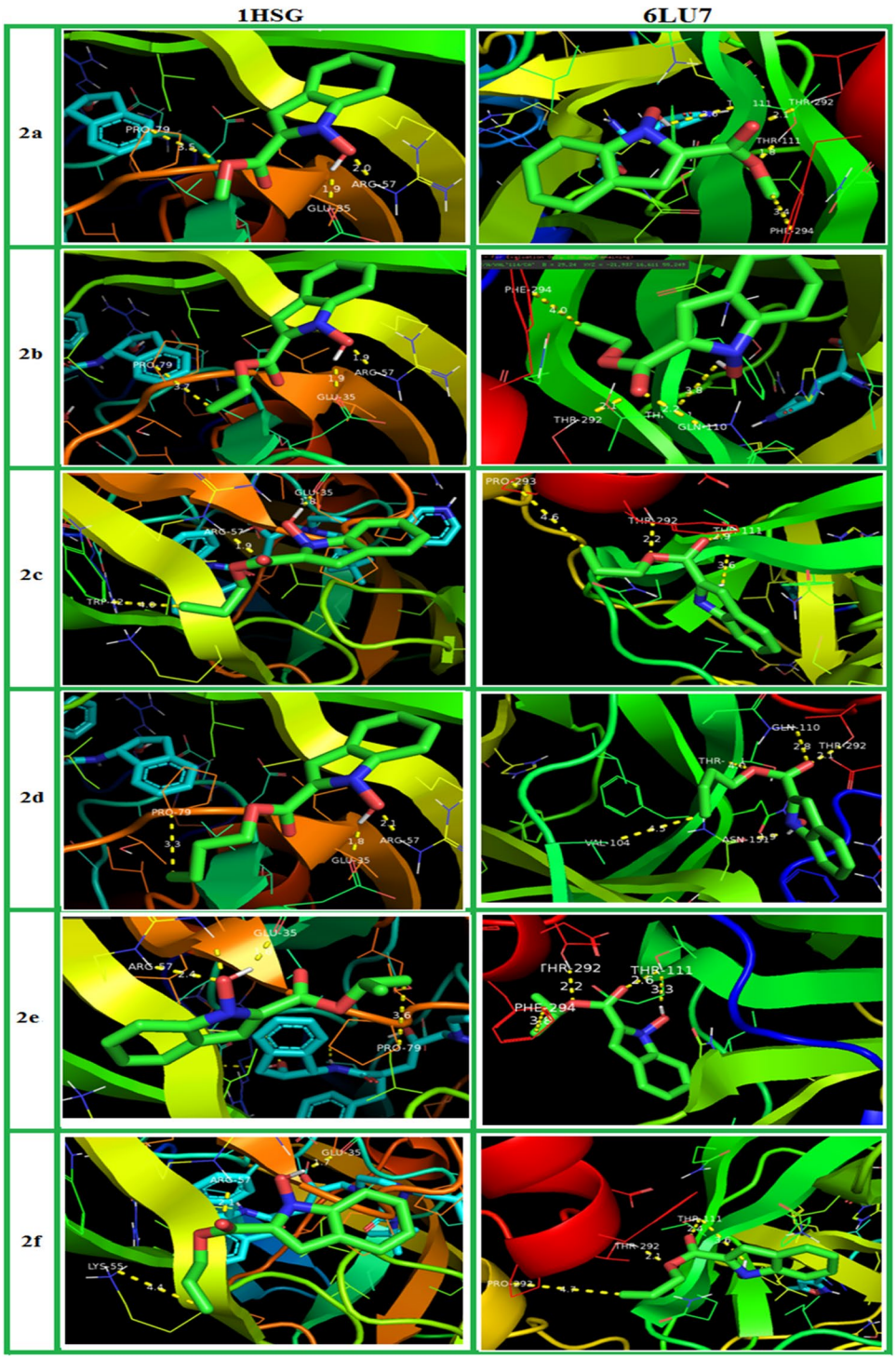

Fig. 7 3D diagrams of the (**2a–2f**) indole derivatives docked into the binding site of the anti-HIV-1 and antiviral proteins

References

1. Shareef M, Rajpurohit H, Sirisha K, Sayeed I (2019) Chem Sel 4:2258–2266
2. Li J, John GC, Webster M (1996) J Nat Prod 59:1157–1158
3. Rhodes S, Short S, Sharma R, Jha KM (2013) J OBC 00:1–3
4. Devi NS, Sreepada D, Manda S (2019) Pharma Innov J 8(1):33–37
5. Saritha Devi N, Srinivas B, Manda S (2019) J Pharm Sci Res 11(3):741–746
6. Zhao Y, Luo Y, Zhu Y, Wang H, Zhou H (2018) Synlett 29:773–778
7. Zhang F, Zhao Y, Sun L, Ding L, Gu Y, Gong P (2011) Eur J Med Chem 46:3149–3157

8. Ahmad A, Dandawate P, Schruefer S, Padhye S (2019). Fazlul Chem Biodiversity. https://doi.org/10.1002/cbdv.(2019)00028IU
9. Wang HX, Ng TB (2002) Comp Biochem Physiol C 132:261–268
10. Ran J-Q, Huang N, Hui Xu, Yang L-M, Lv M, Zheng Y-T (2010) Bioorg Med Chem Lett 20(12):3534–3536
11. Ling-Ling F, Wu-Qing L, Hui XU, Liu-Meng Y, Min LV, Yong-Tang Z (2009) Chem Pharm Bull 57(8):797–800
12. Kelly TA, McNeil DW, Rose JM, David E, Shih CK (1997) J Med Chem 40:2430–2433
13. Medina JR, Arthur SY, Romeril SP, Grant SW, Hong Li WH, Heerding DA, Minthorn E, Mencken T, Atkins C, Liu Q, Rabindran S (2012) Med Chem 55:7193–7207
14. Wagner J, Matt P, Sedrani R, Albert R, Cooke N, Ehrhardt C, Geiser MG, Rummel WS, Strauss A (2009) J Med Chem 52:6193–6196
15. Haishima Y, Kubota K, Manseki J, Jin Y, Sawada T, Inuzuka K, Funabiki M, Matsui J (2018) J Org Chem 83:4389–4401
16. Chen J, Pang Q, Sun Y, Li X (2011) J Org Chem 76:3523–3526
17. (a) Aygun A, Pindur U (2003) Curr Med Chem 10:1113. (b) Gupta L, Talwar A, Chauhan MS (2007) Curr Med Chem 14:1789. (c) Gul W, Hamann MT (2005) Life Sci 78:442. (3) Sheftell FD, Bigal ME, Tepper SJ, Rapaport AM (2004) Expert Rev Neurother 4:199
18. Chicha H, Abbassi N, Rakib EM, Khouili M, El Ammari L, Spinelli D (2013) Tetrahedron Lett 54:1569–1571
19. El Ghozlani M, Chicha H, Abbassi N, Chigr M, El Ammari L, Saadi M, Spinelli D, Rakib EM (2016) Tetrahedron Lett 57:113–117
20. Abbassi N, Rakib EM, Hannioui A, Alaoui M, Benchidmi M, Essassi EM, Geffken D (2011) Heterocycles 83:891–900
21. Abbassi N, Rakib EM, Bouissane L, Hannioui A, Khouili M, El Malki A, Benchidmi M, Essassi EM (2011) Synth Commun 41:999–1005
22. Kouakou A, Chicha H, Rakib EM, Gamouh A, Hannioui A, Chigr M, Viale M (2015) J Sulfur Chem 36:86–95
23. Abbassi N, Rakib EM, Chicha H, Bouissane L, Hannioui A, Aiello C, Gangemi R, Castagnola P, Rosano C, Viale M, Arch M (2014) Pharm Chem Life Sci 347:423–431
24. Abbassi N, Chicha H, Rakib EM, Hannioui A, Alaoui M, Hajjaji A, Geffken D, Aiello C, Gangemi R, Rosano C, Viale M (2015) Eur J Med Chem 2012(57):240–249
25. Kouakou A, Abbassi N, Chicha H, Ammari LE, Saadi M, Rakib EM (2015) Synthesis of Novel Substituted Indazoles via Nucleophilic Substitution of Hydrogen (SNH). The reaction of N-alkyl-7-nitroindazoles with arylaceto-nitriles in basic media is investigated. Heteroat Chem 26(5):374–381
26. Belghiti ME, Benhiba F, Benzbiria N, Chin-Hung L, Echihi S, Salah M, Zeroual A, Karzazi KY, Tounsi A, Abbiche K, Belaaouad S, Elalaoui-Elabdallaoui H, Naimi Y (2022) J Mol Struct 1256(15):132515
27. Dennington R, Keith TA, Millam JM (2016) Semichem Gauss View, Version 6. Shawnee Mission, KS
28. Belghiti ME, Mihit M, Mahsoune A, Elmelouky A, Mghaiouini R, Barhoumi A, Dafali A, Bakasse M, El Mhammedi MA, Abdennouri M (2019) JMRT 8(6):6336–6353
29. Mechbal M, Belghiti ME, Benzbiria N, Chin-Hung L, Kaddouri Y, Karzazi Y, Touzani R, Zertoubi M (2020) J Mol Liq 331(1):115656
30. Belghiti ME, Dafali A, Karzazi Y, Bakass M, Elalaoui-Elabdallaoui H, Lasunkanmie LOO, Ebenso EE (2019) Appl Surf Sci 491(15):707–722
31. Belghiti ME, Echihi S, Mahsoune A, Karzazi Y, Aboulmouhajir A, Dafali A, Bahadur I (2018) J Mol Liq 261:62–75
32. Belghiti ME, Bouazama S, Echihi S, Mahsoune A, Elmelouky A, Dafali A, Emran KM, Hammouti B, Tabyaoui M (2017). Arab J Chem. https://doi.org/10.1016/j.arabjc.2017.12.003
33. Singh I, Al-Wahaibi LH, Srivastava R, Prasad O, Pathak SK, Kumar S, Parveen S, Banerjee MA, El-Emam LA, Sinha L (2020) ACS Omega 5(46):30073–30087
34. Satoh K, Sakagami H, Kurihara T, Motohashi N (1997) Anticancer Res 17(4A):2465–2469
35. Belghiti ME, El Ouadi Y, Echihi S, Elmelouky A, Outada H, Karzazi Y, Jama C, Bentiss F, Dafali A (2020) Surf Interfaces 21:100692
36. Radwan MAA, Ragab EA, Sabry NM, El-Shenawy SM (2007) Bioorg Med Chem 15:3832–3841
37. Mohamed MS, Youns MM, Ahmed R (2014) Med Chem Res. 23:3374–3388
38. Abdel-Gawad H, Mohamed HA, Dawood KM, Badria FAR (2010) Chem Pharm Bull 58:1529–1531
39. Wang H (2002) Comp Biochem Physiol C Toxicol Pharmacol 132:261–268
40. Tantak MP, Gupta V, Nikhil K, Arun V, Singh RP, Jha PN et al (2016) Bioorg Med Chem Lett 26:3167–3171
41. Daisley RW, Shah VK (1984) J Pharm Sci 73:407
42. Piscopo E, Diurno MV, Gogliardi R, Cucciniello M, Veneruso G (1987) Boll Soc Ital Biol Sper 63:827
43. Pandeya SN, Sriram D, Clercq E, De Pannecuque C, Witvrouw M (1998) Indian J Pharm Sci 60:207
44. Sanner MF (1999) J Mol Graphics Mod 17:57–61
45. The PyMOL Molecular Graphics System. Version 1.5.0.4 Schrodinger LLC